Int. J. Electrochem. Sci., 9 **(2014)** 1854 - 1866

International Journal of
ELECTROCHEMICAL
SCIENCE
www.electrochemsci.org

Lithium Ion Migration in Li-Si alloys: From First Principles Studies

H. R. Yao[1], Z. Q. Wang[1], M. S. Wu[1], G. Liu[1], X. L. Lei[1], B. Xu[1,2], J. X. Le[1], C. Y. Ouyang[1,2,]*

[1] Department of Physics, Jiangxi Normal University, Nanchang, 330022, P. R. China
[2] Key Laboratory for Advanced Functional Materials of Jiangxi Province, Nanchang, 330022, P. R. China
[*]E-mail: cyouyang@jxnu.edu.cn

Received: 10 December 2013 / *Accepted:* 7 January 2014 / *Published:* 2 February 2014

Li ion migration dynamics in the bulk and at the surface of Li-Si alloys are investigated from first principles calculations. Vacancy mediated Li migration and interstitial Li migration are considered. Among various phases of Li-Si alloys, we selected Li_1Si_1 and Li_2Si_1 as two typical examples in this work. The vacancy formation energies and the site energies of the interstitial Li are calculated in advance in order to figure out reasonable migration pathways, which are then optimized with nudged elastic band methods. Results shown that Li vacancy diffusion in the bulk phases can be fast, while the intrinsic vacancy formation is difficult. At the Li-Si alloy surfaces, Li migration can be assisted either by Li vacancy or interstitial Li. Li migration at the surface creates vacancies at the surface region and the vacancies can diffuse into the bulk, which in turn enhances the Li diffusion in the bulk region.

Keywords: Lithium ion batteries; Si anode; Li-Si alloys; Li ion migration;

1. INTRODUCTION

Lithium ion batteries attracted widespread attention in both the academic and industrial fields in the past two decades [1]. Silicon is an important candidate as anode material for the next generation lithium ion batteries because of its extremely high theoretical capacity (4200 mAh/g) [2-5]. However, the cycling performance of silicon anode is very poor due to the huge volume change (>300%) during the charging and discharging process [5, 6]. The lithiation/delithiation of the Si anode is accompanied with the structural phase transition between Si crystalline and different kinds of Li-Si alloys [7-9].

There are many papers available in literature focused on the lithiation process of crystalline silicon. The lithiation process of both crystalline and amorphous Si was studied from first principles calculations [10-12]. Chan et al. studied the electrochemical lithiation/delithiation of faceted crystalline

Si from *ab initio* molecular dynamics simulations using slab models [13]. Those studies are mainly concentrated on the structural transition or new phase formation upon lithiation/delithiation, which is one important aspect of the fundamental physics for the application of Si as anode material. On the other hand, the lithium ion migration dynamics is another important physics problem, which is strongly associated with the speed of the structural phase transition and thus the rate performance of the anode material. The importance of the ionic and electronic conductivity at the surfaces and interfaces to the fast charge/discharge performance of a battery has been highlighted [14].

Lithium ion diffusion behavior in crystalline [15, 16] and amorphous [17] Si is also studied from first principles calculations. The lithium migration energy barrier (~0.5 eV) and its dependence on the orientation of the migration pathway and the topology of the amorphous structure are discussed extensively. However, little information concerning lithium ion diffusion behavior in the Li-Si alloy phases are reported in literature, although the Li-Si phases dominate the lithiation/delithiation process of the Si anode. The phase transition between different Li-Si alloys is a process of moving lithium from high Li concentration phases to low Li concentration phases, or a process in a reverse manner. This process is more important to the dynamic performance of the Si anode material than the Li ion migration dynamics in crystalline Si. The phase transition processes between various Li-Si alloys are controlled by the lithium diffusion within the Li-Si alloy and at the phase boundary (interface) area.

Theoretical study and simulation of Li migration in the bulk phases of Li-Si alloys and at the surface/interface can provide fundamental information to understand the lithium ion dynamic process. Comparing with experiment methods, density functional theory (DFT) electronic structure calculations enables us understand these fundamental physics from the atomic level. The purpose of this work is to identify Li migration pathway in the bulk and at the surface of Li-Si alloy theoretically, and reveal the possible diffusion mechanism. Since Li_1Si_1 and Li_2Si_1 phases are two typical and stable structures among various Li-Si alloy phases, we selected them as the object of this study.

2. COMPUTATIONAL DETAILS AND STRUCTURAL PARAMETERS

Density functional theory (DFT) calculations are performed with the Vienna *ab initio* simulation package (VASP) [18, 19]. The interaction between core ion and valence electron are described by the projector augmented wave method (PAW) [20] and the exchange-correlation part is described with the generalized gradient approximation (GGA) by Perdew and Wang (PW91) [21]. The energy cutoff for the expansion of the plane-wave basis set is 450 eV. The atomic positions are fully relaxed and the final forces on all relaxed atoms are less than 0.005 eV/Å. The Monkhorst-Pack [22] scheme ***k***-point sampling has been used for the integration of the Brillouin zone, and the choice of the ***k***-mesh is denser than 0.03 $Å^{-1}$ for all cases in this study. The lithium migration pathway and the corresponding energy barrier are optimized with nudged elastic band (NEB) method [23]. For the simulation of lithium migration at the Li-Si alloys surfaces, we employed the slab models. The slabs are separated from their periodic images by a vacuum layer of ~15Å in thickness. To reproduce the bulk characteristics in the slab model, we fixed half of the atoms at one side and relaxed the atoms at the other side of the slab.

Before studying the behavior of lithium ion, we optimized the structural parameters and the results are listed in Table 1 together with the experimental results. As it is shown, the theoretical lattice parameters are in good agreements with the experimental data, indicating that the computational method and parameters for the calculations are reasonable.

Table 1. Calculated lattice constants and corresponding experimental values for crystalline Li-Si alloys considered in this work.

phases	space group	lattice parameters	
		calculated (this work)	experimental
Li_1Si_1	$I4_1/a$	a=b=9.353, c=5.743 α=β=γ=90°	a=b=9.353, c=5.746 α=β=γ=90° (a)
Li_2Si_1	$R\bar{3}m$	a=7.558, b=4.363, c=6.690 α=β= 90°, γ=112.25°	a=7.70, b=4.41, c=6.56 α=β= 90°, γ=113.4° (b)

3. RESULTS AND DISCUSSION

Generally speaking, there are two possible lithium migration mechanisms in the Li-Si alloys: Li vacancy migration and interstitials Li atom migration. The Li vacancy can be created by removing one Li atom from the perfect lattice, and then the Li vacancy migration can be described by exchanging the positions between one Li ion and the vacancy. Within the vacancy migration mechanism, the vacancy concentration is one important factor to the diffusion coefficient. In a solid, the vacancy concentration is strongly related with the vacancy formation energy. In this work, only monovacancies are considered and the Li vacancy formation energy is defined as $E_{for}=E[Li_{m-1}Si_n]+E[Li_{bcc}]- E[Li_mSi_n]$, where $E[Li_{m-1}Si_n]$ and $E[Li_mSi_n]$ are total energies of the Li-Si alloy supercell with and without one Li vacancy, respectively. $E[Li_{bcc}]$ is the energy of one Li atom in the body centered cubic (bcc) Li metal structure.

For the interstitial Li, we add one Li atom into the perfect lattice of the system and put it at one interstitial site. In doing so, we need to figure out the favorable interstitial sites. We tried different interstitial sites in the lattice and comparing the site energies defined as $E_{Li\text{-}site}=E[Li_{m+1}Si_n]-E[Li_{bcc}]-E[Li_mSi_n]$, where $E[Li_{m+1}Si_n]$ and $E[Li_mSi_n]$ are total energies of the Li-Si alloy supercell with and without one interstitial Li atom, respectively. Similar to the Li vacancy formation energy, the site energy of the interstitial Li atom is also an important factor to the concentration of the interstitial Li atoms in the lattice. Negative site energy implies stable interstitial site. The simulation of the interstitial Li atom migration is carried out by moving it from one stable site to another.

3.1. Li diffusion in Li_1Si_1

3.1.1. Li migration in Li_1Si_1 bulk

From analysis of the symmetry of the Li_1Si_1 crystal structure, we identify that there is only one type of monovacancy site. The Li vacancy formation energy is calculated to be about 3.0 eV according

to the definition above. This is rather high and the concentration of the monovacancy should be very low at room temperature.

Since there is only one type of monovacancy in the Li_1Si_1 crystal structure, the vacancy migration pathway is very simple, and we figured out one migration pathway with shortest migration distance, as shown and numbered as "1-Li_1Si_1" in Fig.1. The optimized energy profile for the vacancy migration in the Li_1Si_1 phase is also given in Fig. 1, from which we can see that the migration energy barrier is about 0.243 eV.

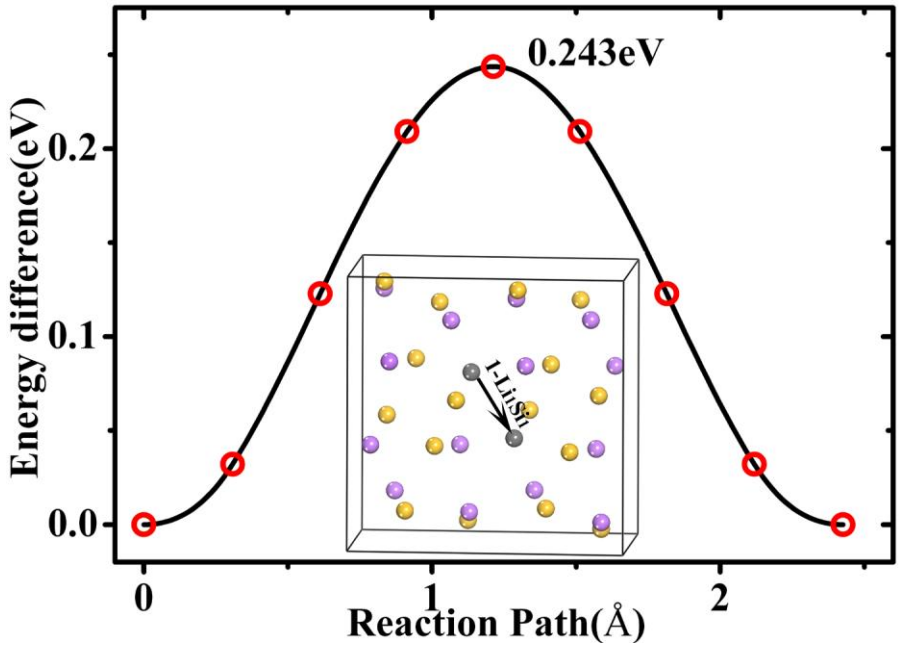

Figure 1. Migration pathways (inset) and energy profile of Li monovacancy migration in Li_1Si_1 bulk. The purple and yellow spheres are Li and Si atoms, respectively. The gray spheres are the Li vacancy positions. The migration pathway is marked with an arrow.

To simulate the interstitial Li migration, we first need to search for and optimize the stable Li interstitial sites. We tried all possible interstitial sites in the lattice and finally we found that there are two types of stable interstitial sites and denoted as "Int-1" and "Int-2" shown in Fig. 2. The site energies are -1.54 eV and -1.15 eV for "Int-1" and "Int-2", respectively. We mention here that the interstitial Li pushes away its nearby atoms and large relaxation is observed around the interstitial Li. Taking into account the symmetry, we considered two independent Li migration pathways as shown in Fig. 2a and numbered as "2-Li_1Si_1" and "3-Li_1Si_1". Fig. 2b and 2c are the corresponding optimized migration energy profiles for pathways "2-Li_1Si_1" and "3-Li_1Si_1". "Int-1" and "Int-2" sites are distribute alternatively along a chain that parallel to the OC direction, and pathways "2-Li_1Si_1" and "3-Li_1Si_1" are for Li migration between and within the OC chain. The results show that the energy barrier for Li migration along the OC chain is lower than the other one. However, the energy barrier value (1.172 eV) is still very high for Li ion migration at room temperatures.

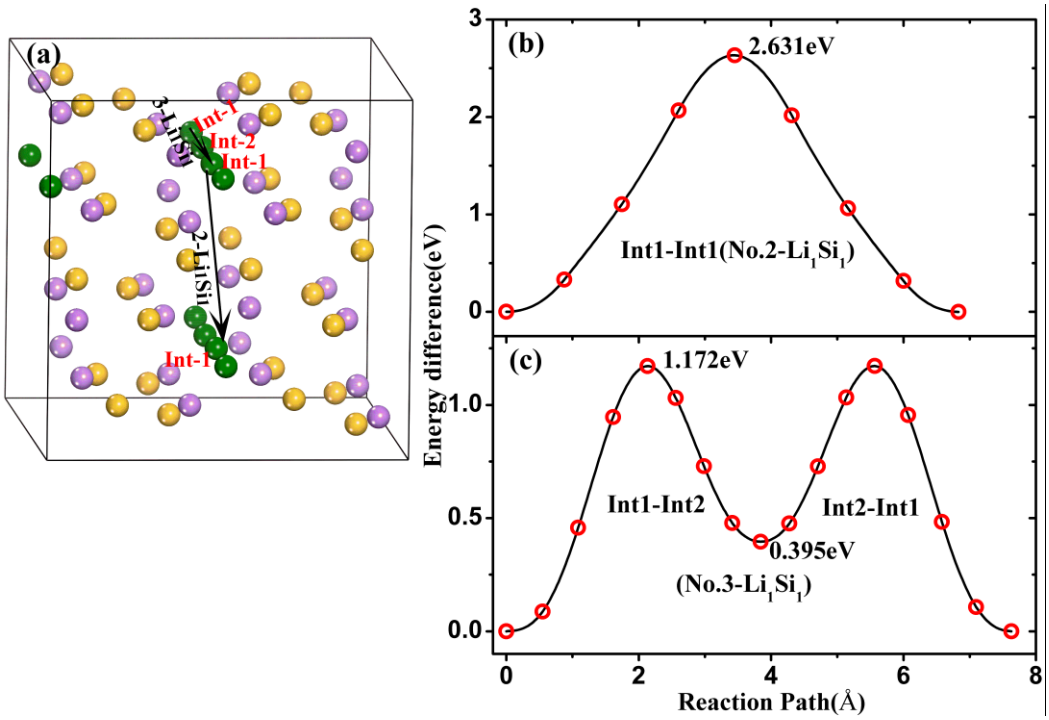

Figure 2. Migration pathways (a) and energy profiles (b and c) of interstitial Li migration in Li_1Si_1 bulk. The purple and yellow spheres are Li and Si atoms respectively and the green spheres are interstitial Li atoms. The migration pathways are marked with arrows.

3.1.2. Li migration at Li_1Si_1 surface

In order to simulate the lithium migration at the surface, we first need to figure out the stable surface model. The stability of a surface can be characterized by the surface energy E_{surf} that can be calculated by:

$$E_{surf} = (E_{slab} - E_{bulk})/(2A)$$

Where E_{slab} is the total energy of the slab, E_{bulk} is the total energy of the corresponding bulk which has the same stoichiometry and atom number with the slab. A is the area of the surface.

In this work, we calculated the surface energies of all low index surfaces including (100), (010), (001), (110), (101), (011) and (111). From the tetragonal structure of the Li_1Si_1 phase as shown in Tab. 1, we can see that the (100) surface is identical to the (010) surface, the (101) surface is identical to the (011) surface. The calculated surface energies are given in Table 2. For all these surfaces, we calculated the surface energies with different terminations, and the results given in Tab. 2 are the surface termination with lowest surface energy. We mention here that for all those surfaces the nonpolar termination has the lowest surface energy. As it is shown in Tab. 2, the surface energy of the (100) surface is substantially lower than the other surfaces. Furthermore, we also tested the thickness of the slab model in order to obtain a reasonable model. We found that the surface energy of the (100) surface calculated with a slab that contains 32 atoms (0.614 J/m²) is very close to that of calculated with a slab that contains 64 atoms (0.607 J/m²). The difference is negligibly small, and therefore the lithium migration at the Li_1Si_1 surface is modeled with the (100) surface in the following of this paper.

Table 2. The surface energies of various low index Li_1Si_1 surfaces.

Surfaces	(100)/(010)	(001)	(110)	(101)/(011)	(111)
E_{surf} (J/m^2)	0.614	0.957	0.941	0.949	0.917

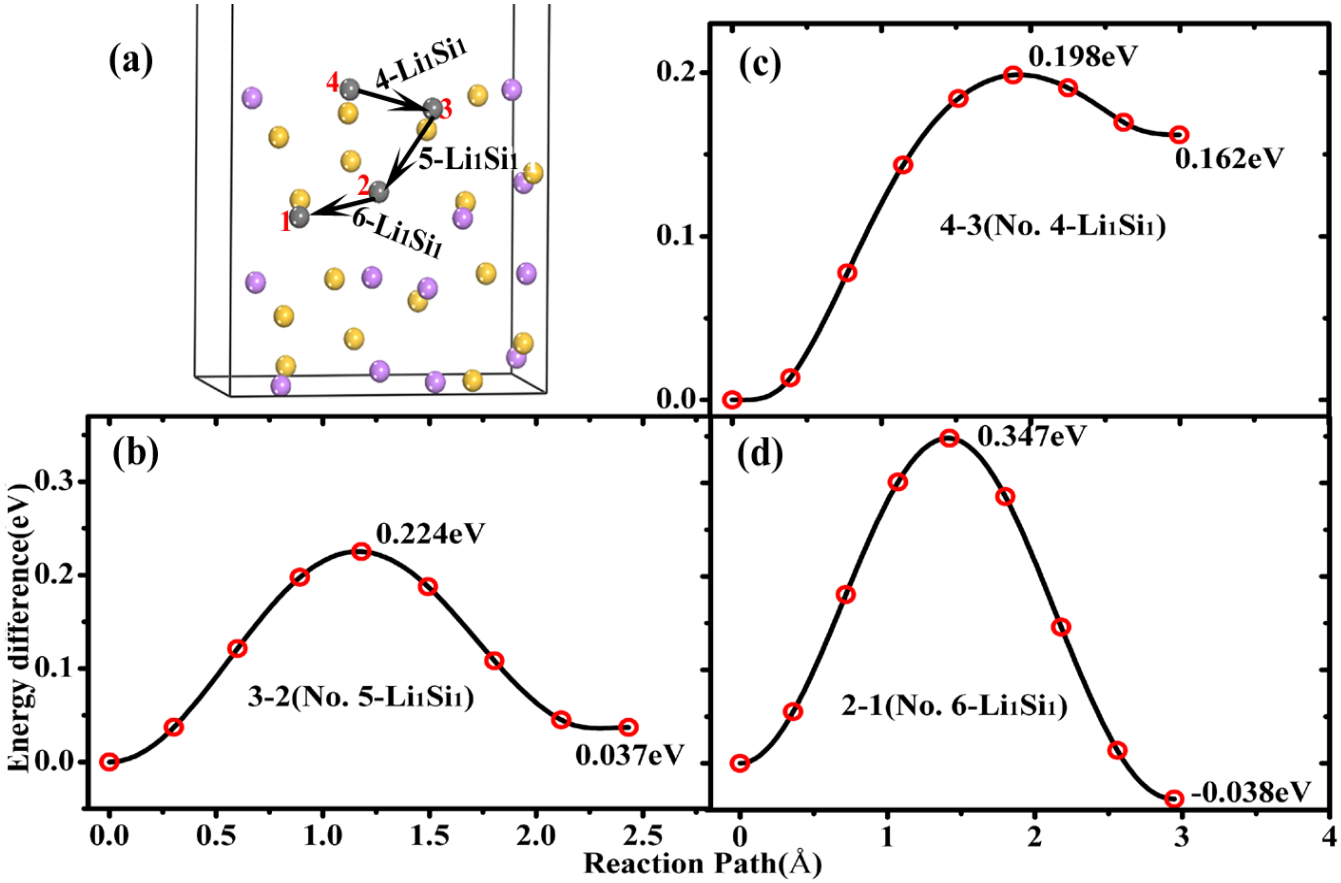

Figure 3. Migration pathways (a) and energy profiles (b to d) of Li vacancy migration at Li_1Si_1 surface region. The purple and yellow spheres are Li and Si atoms respectively and the gray spheres are the Li vacancy positions. The migration pathways are marked with arrows.

Similar to the lithium migration in bulk, we also simulated Li vacancy migration and interstitial Li migration. For vacancy migration at the Li_1Si_1 surface, we selected four vacant sites as numbered 1 to 4 at the surface and subsurface of the Li_1Si_1 (100), as shown in Fig. 3a. The corresponding vacancy formation energies are given in Table 3. We calculated the vacancy migration along pathways from site 4 to 3, site 3 to 2, and site 2 to 1, which are numbered as "4-Li_1Si_1", "5-Li_1Si_1" and "6-Li_1Si_1", respectively in Fig. 3a. The corresponding lithium migration energy barriers are 0.198 eV, 0.224 eV and 0.347 eV, respectively. The energy barrier for Li vacancy migration is relatively low, while the vacancy formation energy is quite high. Therefore, the Li diffusion at the Li_1Si_1 surface through Li vacancy migration mechanism is determined by the vacancy formation.

Table 3. Vacancy formation energies of four different vacancy sites at the Li_1Si_1 (100) surface.

Vacancy site No.	1	2	3	4
E_{for} (eV)	2.957	2.996	2.959	2.797

For interstitial Li migration at the surface, we considered different interstitial sites at the (100) surface and in the subsurface layer. We find that there are only one stable interstitial site at the surface and one stable interstitial site at the subsurface layer, as shown and numbered as "Int-1" and "Int-2" in Fig. 4a. The calculated site energies are -2.190 eV and -1.970 eV for sites "Int-1" and "Int-2", respectively. The site energies for Li at the surface region are obviously lower than that of in the bulk of the Li_1Si_1 phase. This is favorable to the formation of more interstitial Li at the surface region. Fig. 4a also shows the three different migration pathways (numbered as "7-Li_1Si_1" "8-Li_1Si_1" "9-Li_1Si_1") for single interstitial Li migration. Those pathways represent Li migration at the surface and from surface to the subsurface layer. Fig. 4b to 4d show the energy profiles along the optimized Li migration pathways of "7-Li_1Si_1" to "9-Li_1Si_1", respectively. The results show that interstitial Li migration at the surface is allowed (energy barrier 0.432eV) while from bulk to surface is very difficult (energy barrier 1.766 eV).

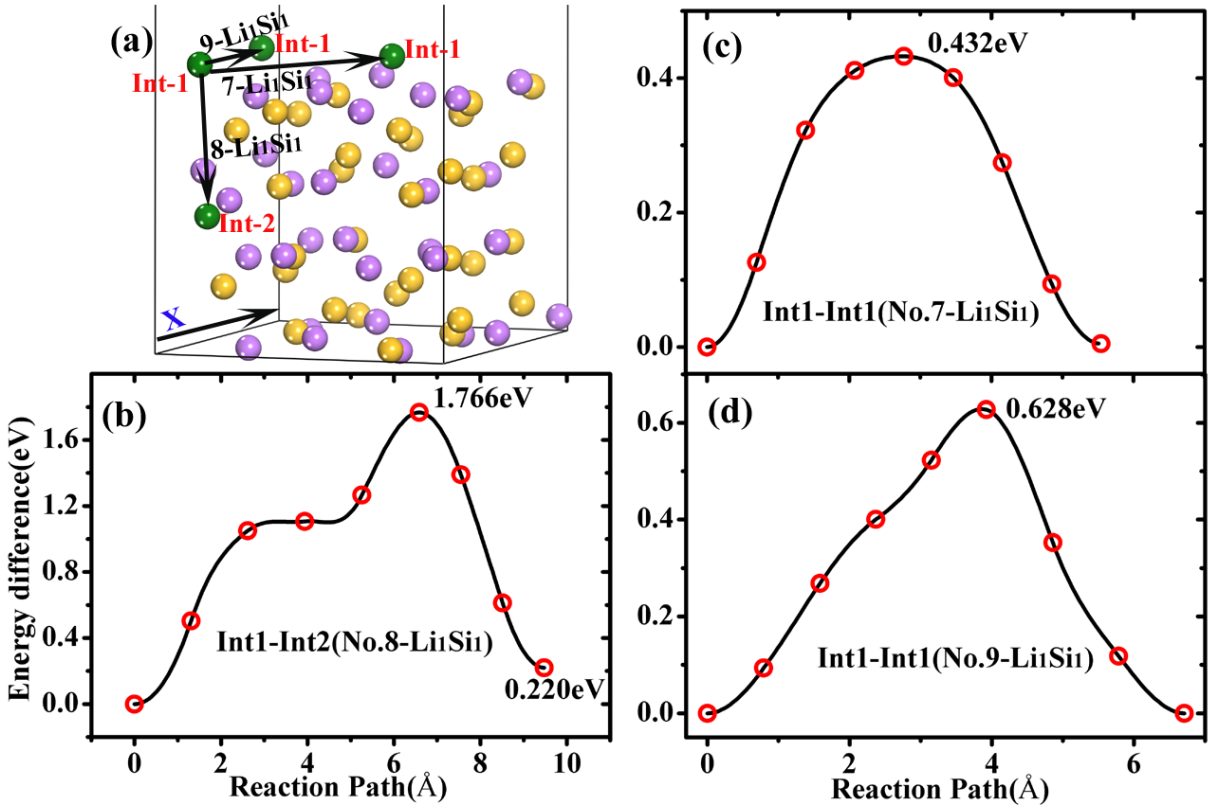

Figure 4. Migration pathways (a) and energy profiles (b to d) of interstitial Li migration at Li_1Si_1 surface region. The purple and yellow spheres are Li and Si atoms respectively and the green spheres are interstitial Li atoms. The migration pathways are marked with arrows.

3.2 Li diffusion in Li_2Si_1

3.2.1 Li migration in the Li_2Si_1 bulk

There are two types of monovacancies in Li_2Si_1 phase as shown and numbered as "1"and "2" in Fig. 5a. The vacancy formation energies are 2.989 eV and 3.013 eV for sites "1" and "2", respectively, very close to that of in the Li_1Si_1 phase. According to the symmetry analysis, we figure out five independent Li vacancy migration pathways in the Li_2Si_1 bulk. Fig. 5a shows these migration pathways schematically and numbered sequentially from "1-Li_2Si_1" to "5- Li_2Si_1". Figs. 5b to 5f are the corresponding energy profiles along the optimized pathways from the NEB calculations. As it can be seen in Fig. 5, the lowest energy barrier is around 0.084 eV (pathway "5-Li_2Si_1"), and the highest energy barrier is about 0.233 eV (pathway "4-Li_2Si_1"). As the Li vacancy migration in the Li_1Si_1 phase, the energy barrier values are low, showing that vacancy migration in Li_2Si_1 bulk can be very fast. Lithium diffusion in the Li_2Si_1 bulk through vacancy migration mechanism is also determined by the vacancy formation and vacancy concentration.

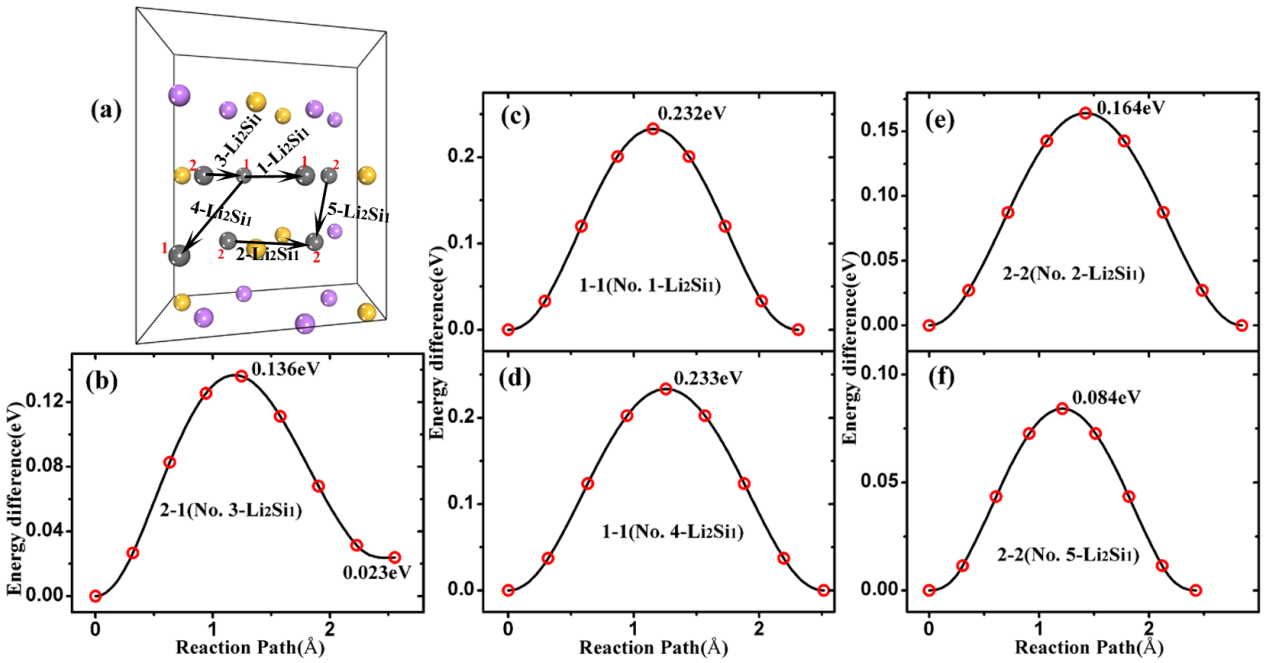

Figure 5. Migration pathways (a) and energy profiles (b to f) of Li monovacancy migration in Li_2Si_1 bulk. The purple and yellow spheres are Li and Si atoms respectively and the gray spheres are the Li vacancy positions. The migration pathways are marked with arrows.

As for interstitial Li migration, we also need to find out the stable interstitial sites and results show that there is only one stable interstitial site (green spheres shown in Fig. 6) in Li_2Si_1 phase. The site energy is -2.555 eV, which is substantially lower than that of in the Li_1Si_1 phase. We figured out two independent pathways (numbered "6-Li_2Si_1" and "7-Li_2Si_1") according to the symmetry. Fig.6 shows that interstitial Li migration between atoms from different layers is allowed (energy barrier 0.294eV) while between atoms in same layer is very difficult (energy barrier 1.638 eV).

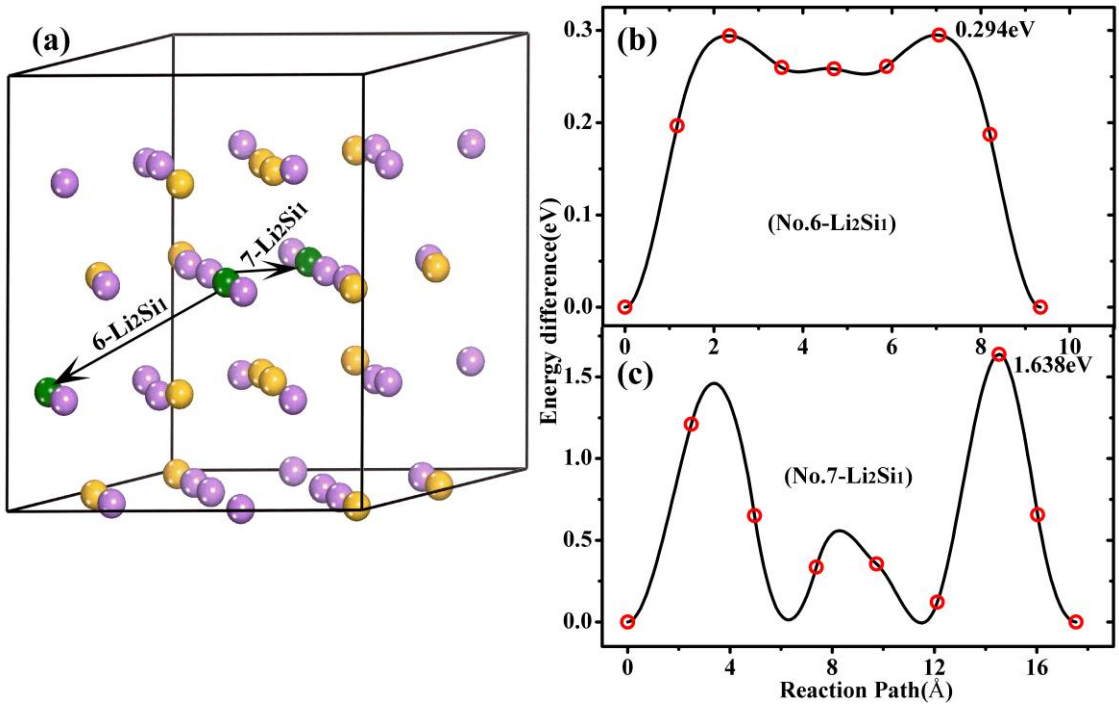

Figure 6. Migration pathways (a) and energy profiles (b and c) of interstitial Li migration in Li_2Si_1 bulk. The purple and yellow spheres are Li and Si atoms respectively and the green spheres are interstitial Li atoms. The migration pathways are marked with arrows.

3.2.3 Li migration at the Li_2Si_1 surfaces

Similar to the Li_1Si_1 phase, we also need to find out the most stable surface of the Li_2Si_1 phase. We calculated the surface energies of all low index surfaces including (100), (010), (001), (110), (101), (011) and (111). The results are given in Table 4, from which we can see that the (001) surface is the most stable one and the following studies are based on the (001) slab model. We also tested the size of the slab model and we find that the model with 24 atoms (shown in Fig. 7a) is accurate enough. The surface energy obtained with the slab containing 24 atoms (0.376 J/m²) is very close to that of with 48 atoms (0.375 J/m²).

Table 4. The surface energies of Li_2Si_1 low index surfaces considered in this work.

Surfaces	(100)	(010)	(001)	(110)	(101)	(011)	(111)
E_{surf} (J/m^2)	0.724	0.651	0.376	0.678	0.704	0.837	0.799

There are one type of Li monovacancy at the Li_2Si_1 (001) surface (vacancy formation energy 2.781 eV) and one type at the subsurface (vacancy formation energy 3.162 eV). To simulate the Li vacancy migration, we select 4 vacancy sites in the slab model and number them as “1” to “4” in Fig 7a. We calculated a sequential pathways for vacancy migration from site “4” to site “3” (numbered as

"8-Li_2Si_1" in Fig 7), site "3" to site "2" (numbered as "9-Li_2Si_1" in Fig 7), and site "2" to site "1" (numbered as "10-Li_2Si_1" in Fig 7). Pathway "9-Li_2Si_1" corresponds to the vacancy migration from surface layer to the subsurface layer. The corresponding energy profiles for vacancies migration along these pathways are given by Fig. 7b to 7d. It is shown that the Li vacancy migration at the Li_2Si_1 (001) surface is about 0.419 eV, which is much lower than that of at the subsurface layer (1.261 eV). On the other hand, the vacancy migration from the subsurface to the surface layer is also very low (0.138 eV). These results show that vacancies in the Li_2Si_1 phase tend to move from the bulk to the surface, which is helpful to the formation of the Li_2Si_1 phase from low Li concentration phases.

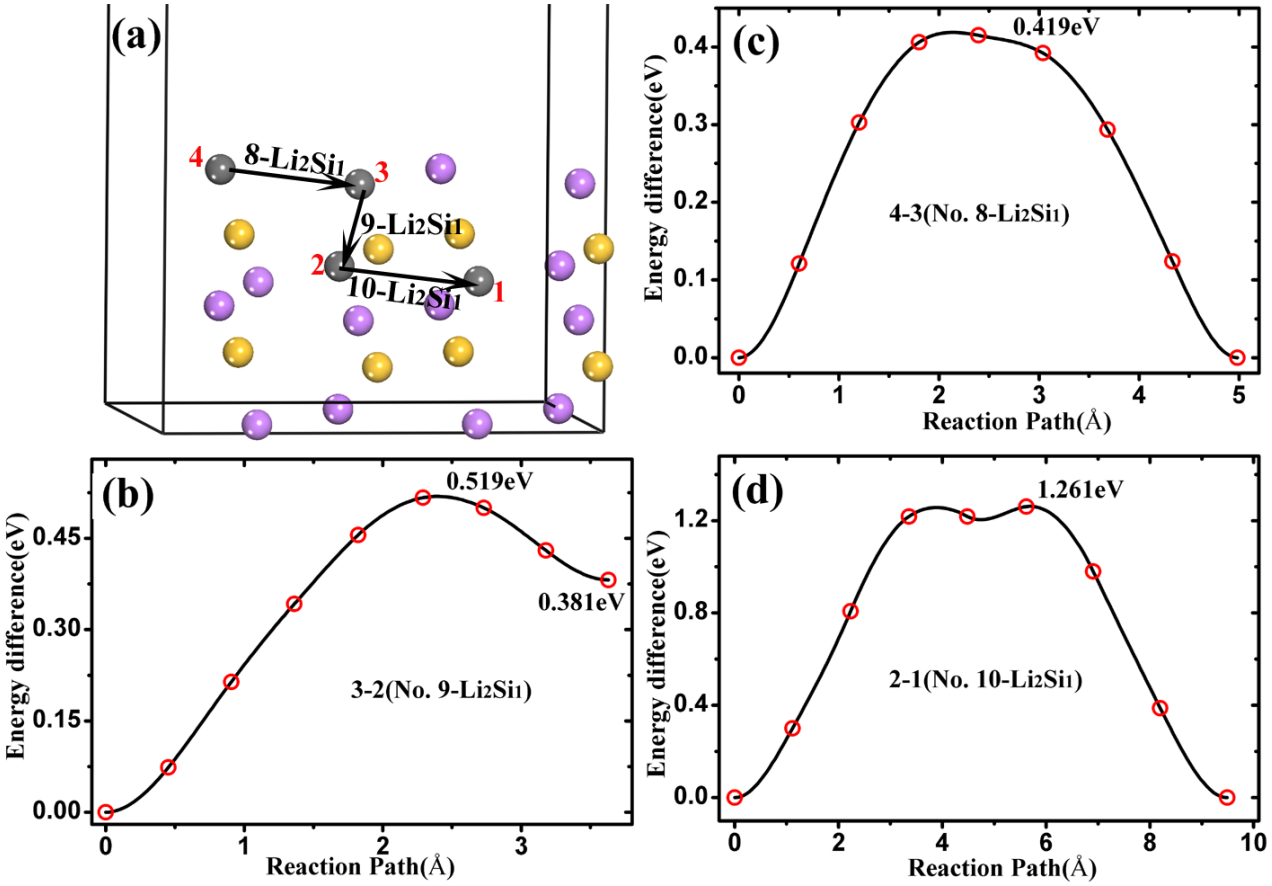

Figure 7. Migration pathways (a) and energy profiles (b to d) of Li monovacancy migration at Li_2Si_1 surface region. The purple and yellow spheres are Li and Si atoms respectively and the gray spheres are the Li vacancy positions. The migration pathways are marked with arrows.

At the Li_2Si_1 (001) surface we can figure out only one stable Li interstitial site (site energy -1.901 eV) shown as green spheres in Fig. 8a. Li at other sites will move to the stable site upon relaxation. Fig. 8a shows two different migration pathways (numbered as "11-Li_2Si_1" and "12-Li_2Si_1") for single interstitial Li migration. Fig. 8b and 8c show the energy profiles along the optimized Li migration pathways of "11-Li_2Si_1" and "12-Li_2Si_1", respectively. The results show that the lowest energy barrier of interstitial Li migration at the surface is about 0.835 eV.

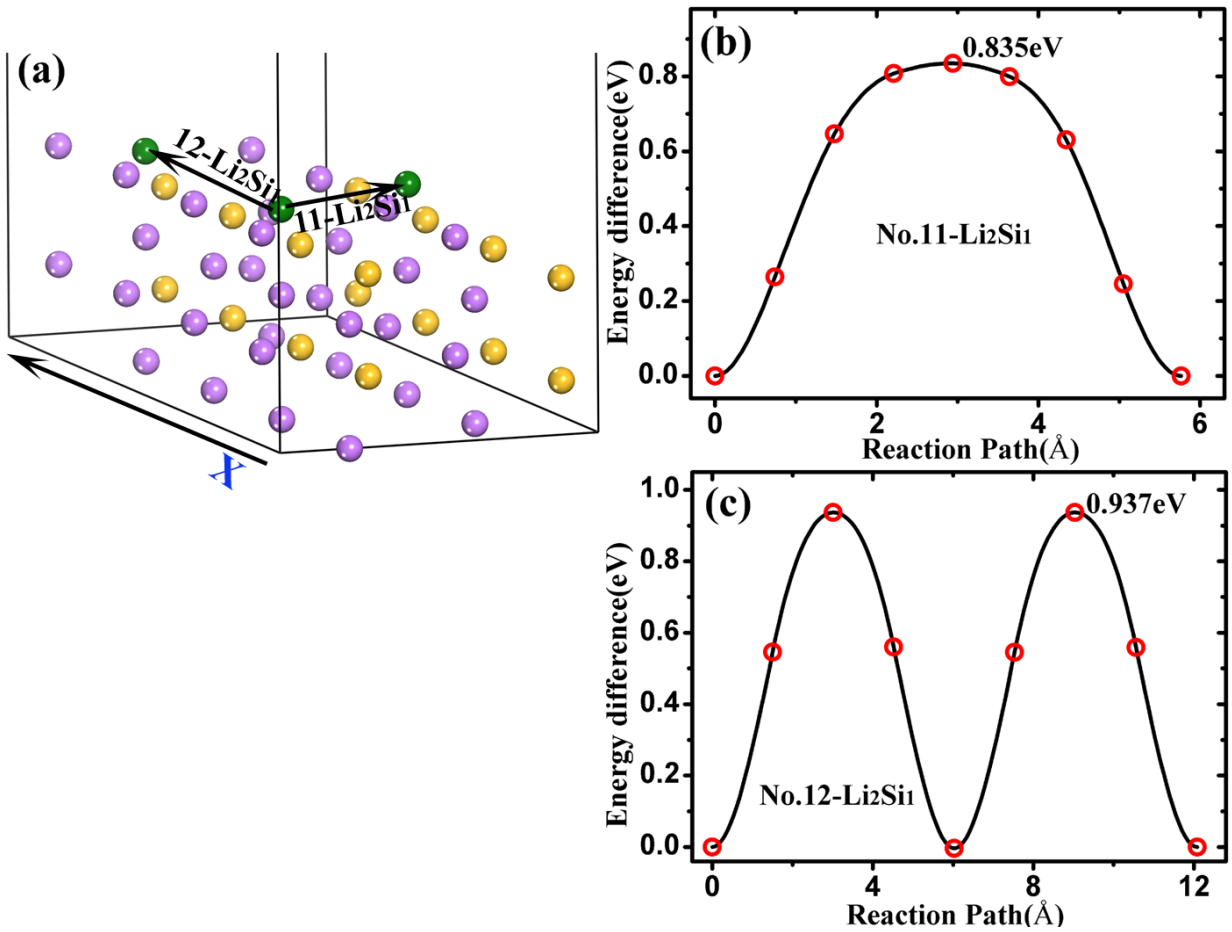

Figure 8. Migration pathways (a) and energy profiles (b and c) of interstitial Li migration at Li_2Si_1 surface region. The purple and yellow spheres are Li and Si atoms respectively and the green spheres are interstitial Li atoms. The migration pathways are marked with arrows.

3.3. Further discussions on Li diffusion in Li-Si alloys

The above results give only basic information on the Li diffusion in Li-Si alloy. The hopping mode and the energy barriers are helpful to the understanding of the Li diffusion mechanism. However, it is not convenient for the comparison to the experimental observations, in which the diffusion coefficient is more relevant. In order to give direct comparison to the experiments, we need to evaluate the diffusion coefficient from the calculated energy barriers.

We assume that the Li diffusion is in a hopping mechanism. From the transition state theory [26], we can calculate the hopping rate $\Gamma = \nu_0 \exp(-E_a / k_B T)$, where ν_0 is the Li vibration frequency and Ea is the Li migration energy barrier, k_B and T are the Boltzmann constant and absolute temperature. We can also assume the Li diffusion occurs within the lattice gas model [27], and the diffusion coefficient can be obtained by $D=\Gamma \times l^2$, where l is the hopping distance. The vibration frequency ν_0 is general in the range of several THz. For simplicity, we can take the vibration frequency ν_0 to be 1 THz. With these models and assumptions, we can calculate the diffusion coefficient that can be directly comparable to the experiments. For example, the energy barrier for Li vacancy migration in the Li_1Si_1 bulk is 0.243 eV, the corresponding diffusion coefficient is evaluated to be ~10^{-7} cm^2/S in magnitude.

4. SUMMARY AND CONCLUSIONS

In summary, Li ion diffusion behaviors in two typical Li-Si alloys Li_1Si_1 and Li_2Si_1 have been studied through first principles calculations. The Li vacancy migration and interstitial Li migration have been studied in the bulk phases and at the stable surfaces of the two alloy phases. The Li migration pathways have been identified and optimized and the corresponding energy barriers have been calculated. Results show that Li vacancy migration in the bulk phases have relatively low energy barrier, while the vacancy formation energy in the bulk phase is relatively high. This indicates that Li diffusion in the bulk phases of the Li-Si alloys can be fast if there are enough Li vacancies available in the bulk. Direct formation of the vacancy in the bulk is not easy at room temperature since the vacancy formation energy is high, but vacancies can be formed indirectly through Li extraction at the surfaces or phase boundary region and diffuses from the surface area to the bulk. At the surfaces, the Li can be extracted or removed through either vacancy assisted migration or interstitial Li migration, because the energy barrier of Li migration through those mechanisms are relatively low at the surfaces. Interstitial Li migration in the bulk phases is not easy due to the relatively high energy barriers. In the Li_2Si_1 phase, interstitial Li migration is one-dimensional because only one migration pathway is allowed and has relatively low energy barrier. However, interstitial Li migration at the surfaces have moderate low energy barrier, indicating that Li diffusion at the surface area can also be assisted by the interstitial Li migration mechanism. Therefore, we can conclude that the Li diffusion in the Li-Si alloys have been dominated by the Li vacancy migration in the bulk phases, while the vacancy formation in the bulk is controlled by the surface Li diffusion, which can be assisted by either Li vacancy migration or interstitial Li migration.

ACKNOWLEDGEMENT
Thanks to the support of Natural Science Foundation of China under Grant Nos. 11234013 and 11264014 and Natural Science Foundation of Jiangxi Province under Grant No. 20133ACB21010. C. Y. Ouyang is also supported by the “Gan-po talent 555” Project of Jiangxi Province.

References

1. J. M. Tarascon, M. Armand, *Nature.* 414 (2001) 359.
2. X. H. Liu, J. W. Wang, S. Huang, F. F. Fan, X. Huang, Y. Liu, S. Krylyuk, J. Yoo, S. A. Dayeh, A. V. Davydov, S. X. Mao, S. T. Picraux, S. L. Zhang, J. Li, T. Zhu, J. Y. Huang, *Nature Nanotech.* 7 (2012) 749.
3. S. Misra, N. Liu, J. Nelson, S. S. Hong, Y. Cui, M. F. Toney, *ACS Nano*. 6 (2012) 5465.
4. K. Kang, H. S. Lee, D. W. Han, G. S. Kim, D. H. Lee, G. Lee, Y. M. Kang, M. H. Jo, *Appl. Phys. Lett.* 96 (2010) 053110.
5. U. Kasavajjula, C. Wang, A. J. Appleby, *J. Power Sources* 163 (2007) 1003.
6. H. Wu, Y. Cui, Nano Today 7 (2012) 414.
7. H. Li, X. Huang, L. Chen, G. Zhou, Ze. Zhang, D. Yu, Y. J. Mo, N. Pei, *Solid State Ionics* 135 (2000) 181.
8. P. Limthongkul, Y. I. Jang, N. J. Dudney, Y. M. Chiang, *Acta Mater*. 51 (2003) 1103.
9. C. J. Wen, R. A. Huggins, *J. Solid State Chem*. 37 (1981) 271.
10. V. L. Chevrier, J. R. Dahn, *J. Electrochem. Soc*. 157 (2010) A392.

11. J. M. Huang, Z. Q. Wang, X. Gong, M. S. Wu, G. Liu, J. X. Liang, H. B. Cao, F. J. Tang, M. S. Lei, B. Xu, C. Y. Ouyang, *Int. J. Electrochem. Sci*. 8 (2013) 5643.
12. V. L. Chevrier, J. W. Zwanziger, J.R. Dahn, *J. Alloys Compd*. 496 (2010) 25.
13. M. K. Y. Chan, C. Wolverton, J. P. Greeley, *J. Am. Chem. Soc*. 134 (2012) 14362.
14. J. Maier, Nat. Mater. 4 (2005) 805.
15. W. H. Wan, Q. F. Zhang, Y. Cui, E. G. Wang, *J. Phys.: Condens. Matter*. 22 (2010) 415501.
16. Q. F. Zhang, Y. Cui, E. G. Wang, *J. Phys. Chem*. C 115 (2011) 9376.
17. G. A. Tritsaris, K. J. Zhao, O. U. Okeke, E. Kaxiras, *J. Phys. Chem*. C 116 (2012) 22212.
18. G. Kresse, J. Hafner, *Phys. Rev*. B 48 (1993) 13115.
19. G. Kresse, J. Furthmüller. *Phys. Rev*. B 54 (1996) 11169.
20. P. E. Blöchl, *Phys. Rev*. B 50 (1994)17953.
21. Y. Wang, J.P. Perdew, *Phys. Rev*. B 44 (1991) 13298.
22. H. J. Monkhorst, J.D. Pack, *Phys. Rev*. B 13 (1976) 5188.
23. G. Henkelman, B. P. Uberuaga, H. Jónsson, *J. Chem. Phys*. 113 (2000) 9901.
24. L. A. Stearns, J. Gryko, J. Diefenbacher, G. K. Ramachandran, P.F. McMillan, *J. Solid State Chem*. 173 (2003) 251.
25. H. Axel, H. Schäfer, A. Weiss, *Angew. Chem*. 77 (1965) 379.
26. G. H. Vineyard, *J. Phys. Chem. Solids* 3 (1957) 121.
27. R. Kutner, *Phys. Lett. A* 81(1981) 239.